ChemComm

RSC Publishing

COMMUNICATION

View Article Online
View Journal | View Issue



Cite this: *Chem. Commun.*, 2013, **49**, 6773

Received 30th April 2013,
Accepted 6th June 2013

DOI: 10.1039/c3cc43196g

www.rsc.org/chemcomm

# Low-energy regeneration and high productivity in a lanthanide–hexacarboxylate framework for high-pressure $CO_2$–$CH_4$–$H_2$ separation†

Yabing He,*[a] Hiroyasu Furukawa,[b] Chuande Wu,[c] Michael O'Keeffe,[d] Rajamani Krishna*[e] and Banglin Chen*[f]

**A porous lanthanide–organic framework UTSA-62a of a jjt-a topology has been synthesized from a hexacarboxylate and structurally characterized, exhibiting significant potential for use in $CO_2$–$CH_4$–$H_2$ separation ($H_2$ purification) processes with high productivities and low regeneration costs when operating at high pressure and room temperature.**

Metal–organic frameworks (MOFs) or porous coordination polymers have emerged as an exceptionally versatile class of porous materials. By bridging metal centers with appropriate polyfunctional organic linkers, MOF materials can incorporate both tunable pore size/shape and a modifiable pore surface, which offer great promise for a variety of applications, including gas storage, separation, catalysis, chemical sensing and drug delivery.[1,2]

Research on porous MOFs for carbon capture has mainly focused on the post-combustion $CO_2$ capture under low pressure, while porous MOFs for the pre-combustion $CO_2$ capture, and thus $H_2$ purification under high pressure, have not been extensively explored.[3] The well known MgMOF-74 has been comprehensively examined for $H_2$ purification.[3a,b] Studies have shown that this MOF does exhibit high separation capacity for $H_2$ purification; however, the strong interactions between the framework and carbon dioxide lead to the very high regeneration energy costs. It is highly demanding to develop porous MOF materials which not only exhibit high separation capacity, but also have low regeneration energy costs for such an industrially important process.

We have been pursuing porous MOFs for gas storage and separation over the past several years.[4] A variety of different metal-containing secondary building units (SBUs) and multicarboxylate organic linkers have been utilized to optimize the pore space for gas storage and to tune the pore/cage sizes for gas separation. The ideal porous MOFs for $H_2$ purification should have moderately high porosity and weak interactions with carbon dioxide. Herein, we report a new MOF $Yb_3O(H_2O)_3(L)(NO_3)$ (**UTSA-62a**) constructed from $[Yb_3O(O_2C)_6]$ clusters and dendritic hexacarboxylate organic linkers for such a purpose.

The organic linker $H_6L$ was readily synthesized by Suzuki coupling of 1,3,5-tri(3,5-dibromophenyl)benzene and 4-(methoxycarbonyl)phenyl boronic acid followed by hydrolysis and acidification in good yield. A solvothermal reaction between $H_6L$ and $Yb(NO_3)_3{\cdot}5H_2O$ in *N*,*N*-dimethylacetamide (DMA) in the presence of a small amount of water at 100 °C afforded colorless block-shaped crystals of **UTSA-62** with an empirical formula of $Yb_3O(H_2O)_3(L)(NO_3){\cdot}xG$ (G represents non-coordinated solvent molecules). The structure was determined using single-crystal X-ray diffraction analysis, and the phase purity of the bulk material was confirmed using powder X-ray diffraction (PXRD, Fig. S1, ESI†). Thermogravimetric analysis (TGA) shows that **UTSA-62** can be thermally stable up to 400 °C under a nitrogen atmosphere (Fig. S2, ESI†).

Single-crystal X-ray crystallographic studies reveal that **UTSA-62** crystallizes in a hexagonal space group $P\bar{6}2c$.‡ The asymmetric unit contains half of the Yb(III) ion, one sixth of the deprotonated ligand, one sixth of the $\mu_3$-oxygen atom and half of the terminal water molecule. The unique Yb1 atom and water oxygen atom O4 lie on a mirror plane, and the deprotonated L ligand and the $\mu_3$-oxygen atom O3 have the crystallographically imposed $3_2$ symmetry. Each Yb ion coordinates to six oxygen atoms from four carboxylate groups of L ligands, one terminal water and a $\mu_3$-oxygen atom. Three Yb ions are joined by six carboxylate groups and a $\mu_3$-oxygen atom to form a 6-connected trigonal prismatic SBU $[Yb_3O(O_2C)_6]$. Each ligand links to six

[a] *College of Chemistry and Life Sciences, Zhejiang Normal University, Jinhua 321004, China. E-mail: heyabing@gmail.com*
[b] *Department of Chemistry, University of California, Materials Sciences Division, Lawrence Berkeley National Laboratory, Berkeley, California 94720, USA*
[c] *Department of Chemistry, Zhejiang University, Hangzhou 310027, China*
[d] *Department of Chemistry and Biochemistry, Arizona State University, Tempe, Arizona 85287, USA*
[e] *Van't Hoff Institute for Molecular Sciences, University of Amsterdam, Science Park 904, 1098 XH Amsterdam, The Netherlands. E-mail: r.krishna@nva.nl*
[f] *Department of Chemistry, University of Texas at San Antonio, One UTSA Circle, San Antonio, Texas 78249-0698, USA. E-mail: banglin.chen@utsa.edu; Fax: +1-210-458-7428*

† Electronic supplementary information (ESI) available: Synthesis and characterization of the organic linker and **UTSA-62**, PXRD, TGA, NMR, FTIR, sorption isotherms, IAST and breakthrough calculations, fitting parameters for **UTSA-62a**. CCDC 935253. For ESI and crystallographic data in CIF or other electronic format see DOI: 10.1039/c3cc43196g

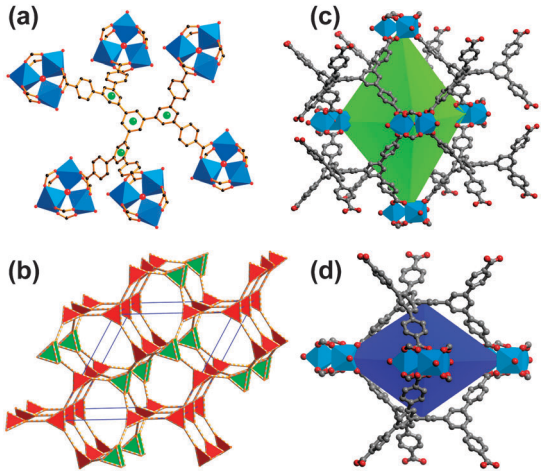


**Fig. 1** Single-crystal X-ray structure of **UTSA-62** showing (a) the coordination environment of the organic building block, (b) the framework topology of **jjt-a**, and (c and d) two kinds of polyhedral cages A and B.

SBUs and serves as a 6-connected node (Fig. 1a), generating a (6,6)-connected binodal network structure of **nia** topology.[5] However, one should recognize the 3-coordinated (3-c) branch points of the hexatopic linker explicitly as there are several distinct ways of replacing the octahedral node of the basic net **nia**. In this case, the derived net is **jjt** shown in Fig. 1b in augmented form (*i.e.* vertices replaced by the vertex figures – triangles and trigonal prisms). There exist two types of trigonal bipyramid cages (cages A and B): cage A is formed by five SBUs as vertices and six ligands as faces with the dimension of *ca.* 15 Å (Fig. 1c), measured by fitting a sphere from the centroid of the cage to the van der Waals surface of its walls; cage B is formed by three SBUs and two ligands with a dimension of *ca.* 14 Å (Fig. 1d). Each cage A is surrounded by three cages B *via* the sharing of tetragonal windows and *vice versa*.

In order to establish the permanent porosity, the as-synthesized sample was guest-exchanged with dry acetone, and then activated using the supercritical $CO_2$ drying method to remove all solvent molecules. The permanent porosity of activated **UTSA-62a** was confirmed by a $N_2$ sorption isotherm. As shown in Fig. S3, ESI,† the $N_2$ sorption isotherm shows type-I adsorption behaviour, characteristic of microporous materials with a Brunauer–Emmett–Teller (BET) surface area of 2190 $m^2\ g^{-1}$ (Fig. S4, ESI†). This is one of the most porous lanthanide–organic frameworks ever reported so far (Table S4, ESI†). Apparently, both the robust $[Yb_3O(O_2C)_6]$ cluster and dendritic hexacarboxylate organic linker play a role in stabilizing the framework. The total pore volume calculated from the maximum amount of $N_2$ adsorbed is 0.91 $cm^3\ g^{-1}$.

Given the high porosity of **UTSA-62a**, we examined the high-pressure $CO_2$, $CH_4$ and $H_2$ adsorption up to 8 MPa using a HPA-100 volumetric high-pressure analyzer. All isotherms show typical type-I behavior with good reversibility (Fig. 2 and Fig. S8, ESI†). The $H_2$ adsorption isotherm of **UTSA-62a** shows a maximum excess uptake of 4.6 wt% at 3.8 MPa and 77 K (Fig. S8, ESI†). By using the $N_2$-derived pore volume and the bulk phase density of $H_2$, the total $H_2$ uptake at 77 K and 8 MPa was calculated to be 6.3 wt%, which is moderate. At 298 K and 8 MPa, the total $H_2$ uptake decreases to 1.0 wt% (Fig. 2). **UTSA-62a** shows excess

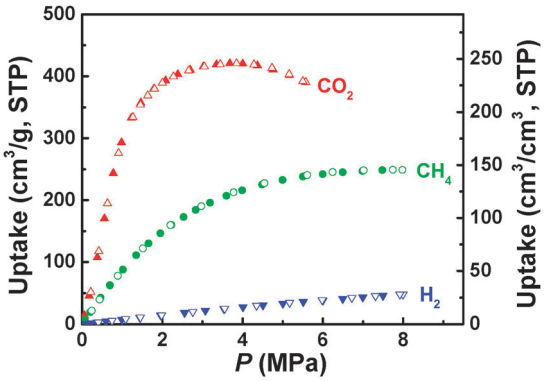


**Fig. 2** Excess high-pressure $CO_2$, $CH_4$ and $H_2$ sorption isotherms of **UTSA-62a** at 298 K. Filled and open symbols represent adsorption and desorption data, respectively.

and total $CH_4$ uptakes of 121 and 139 $cm^3$(STP) per $cm^3$, respectively, at 3.5 MPa and 298 K. The total methane uptake can increase to 189 $cm^3$(STP) per $cm^3$ at 298 K and 8 MPa. The total $CO_2$ adsorption reaches 47.6 wt% (270 $cm^3$(STP) per $cm^3$) at 298 K and 8 MPa.

The higher $CO_2$ and $CH_4$ adsorption capacities of **UTSA-62a** prompted us to examine the potential of **UTSA-62a** for high-pressure $CO_2$–$CH_4$–$H_2$ separation ($H_2$ purification). In order to establish the feasibility of this separation, we performed IAST (Ideal Adsorbed Solution Theory) and breakthrough calculations for the separation of a 30/20/50 $CO_2$–$CH_4$–$H_2$ gas mixture,[6] which is likely to be encountered in industrial practice. As shown in Fig. 3a, for a 30/20/50 $CO_2$–$CH_4$–$H_2$ ternary mixture under isothermal conditions at 298 K and a total pressure of 5.0 MPa at the inlet of the adsorber packed with **UTSA-62a**, the hydrogen breaks through earliest, and therefore it is possible to recover pure hydrogen from this 3-component mixture during the adsorption cycle.

We compared the performance of **UTSA-62a** with the widely used zeolites NaX and LTA-5A and the well-examined MOFs MgMOF-74, Cu-TDPAT, Cu-BTC, MIL-101 and UTSA-40a for the high-pressure $H_2$ purification. The pressure dependent $H_2$ productivities from 0.1 MPa to 6.0 MPa are shown in Fig. 3b, in which the produced $H_2$ is more than 99.95% pure. The productivities of **UTSA-62a** are moderately high. In fact, at the highest pressure of 6.0 MPa, the $H_2$ productivity of **UTSA-62a** is only about 20% lower than those of the best performing MOFs ever reported (MgMOF-74, CuBTC and CuTDPAT) for $H_2$ purification.

Another very important consideration for such an industrially significant separation is the regeneration cost. Since the isosteric heat of adsorption of $CO_2$ is the lowest for **UTSA-62a**, as compared to all other adsorbents (Fig. 4), the regeneration cost can be expected to be less than that of MgMOF-74, CuBTC, and CuTDPAT, thus leading to significant energy saving. This reduced regeneration cost could more than offset the slightly low $H_2$ productivity of **UTSA-62a** relative to MgMOF-74, CuBTC, and CuTDPAT at high pressure. Such low isosteric heats of adsorption of $CO_2$ are attributed to the highly porous structure and the lack of specific binding sites on the pore surfaces for their interactions with $CO_2$.

 

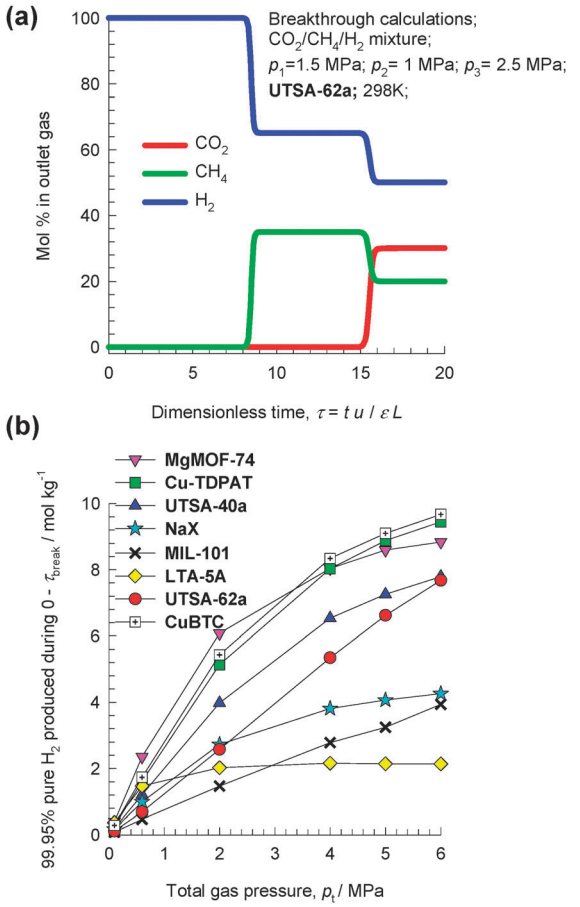


**Fig. 3** (a) Transient breakthrough of a 30/20/50 $CO_2$–$CH_4$–$H_2$ mixture in an adsorber packed with **UTSA-62a**, maintained under isothermal conditions at 298 K and 5.0 MPa. (b) Influence of operating pressure on the number of moles of 99.95+% pure $H_2$ produced per kg of adsorbent material from a 30/20/50 $CO_2$–$CH_4$–$H_2$ mixture at 298 K.

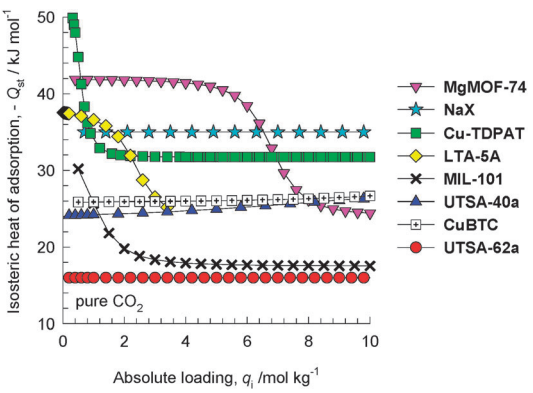


**Fig. 4** Comparison of isosteric heats of $CO_2$ adsorption in **UTSA-62a** with the reported MOFs. The calculations are based on the use of the Clausius–Clapeyron equation.

In summary, we realized a highly porous lanthanide–organic framework **UTSA-62** from a dendritic hexacarboxylate. Both the robust $[Yb_3O(O_2C)_6]$ cluster and dendritic hexacarboxylate organic linker play crucial roles in stabilizing the framework. The high porosity can secure its high $H_2$ productivities, while the low isosteric heats of adsorption of $CO_2$ can minimize the regeneration costs, for $H_2$ purification at high pressure. **UTSA-62** is a very unique MOF material for this industrially important application in which both the productivities and regeneration costs can be equally considered. Given the richness of MOF chemistry, some even more promising MOF materials (higher productivities and/or lower regeneration costs) for $H_2$ purification will be targeted in the near future.

## Notes and references

‡ Crystal data for **UTSA-62:** $C_{122}H_{180}N_{15}O_{39}Yb_3$, $M$ = 2999.93, hexagonal, space group $P\bar{6}2c$, $a = b$ = 19.848 Å, $c$ = 27.853 Å, $V$ = 9502.5 Å$^3$, $Z$ = 2, $D_c$ = 1.048 g cm$^{-3}$, $\mu$(Cu-K$_\alpha$) = 3.126 mm$^{-1}$, $F$(000) = 3078, final $R_1$ = 0.0327 for $I > 2\sigma(I)$, w$R_2$ = 0.0866 for all data, GoF = 1.103. CCDC 935253.

1 (*a*) Y. He, W. Zhou, R. Krishna and B. Chen, *Chem. Commun.*, 2012, **48**, 11813; (*b*) X. Lin, N. R. Champness and M. Schröder, *Top. Curr. Chem.*, 2010, **293**, 35; (*c*) J.-R. Li, J. Sculley and H.-C. Zhou, *Chem. Rev.*, 2012, **112**, 869; (*d*) K. Sumida, D. L. Rogow, J. A. Mason, T. M. McDonald, E. D. Bloch, Z. R. Herm, T.-H. Bae and J. R. Long, *Chem. Rev.*, 2012, **112**, 724; (*e*) H. Wu, Q. Gong, D. H. Olson and J. Li, *Chem. Rev.*, 2012, **112**, 836; (*f*) L. Ma, C. Abney and W. Lin, *Chem. Soc. Rev.*, 2009, **38**, 1248; (*g*) Y. Cui, Y. Yue, G. Qian and B. Chen, *Chem. Rev.*, 2012, **112**, 1126; (*h*) B. Chen, S. Xiang and G. Qian, *Acc. Chem. Res.*, 2010, **43**, 1115; (*i*) L. E. Kreno, K. Leong, O. K. Farha, M. Allendorf, R. P. V. Duyne and J. T. Hupp, *Chem. Rev.*, 2012, **112**, 1105; (*j*) P. Horcajada, R. Gref, T. Baati, P. K. Allan, G. Maurin, P. Couvreur, G. Férey, R. E. Morris and C. Serre, *Chem. Rev.*, 2012, **112**, 1232; (*k*) S. Horike, S. Shimomura and S. Kitagawa, *Nat. Chem.*, 2009, **1**, 695; (*l*) R. Banerjee, A. Phan, B. Wang, C. Knobler, H. Furukawa, M. O'Keeffe and O. M. Yaghi, *Science*, 2008, **319**, 939.

2 (*a*) P. Nugent, Y. Belmabkhout, S. D. Burd, A. J. Cairns, R. Luebke, K. Forrest, T. Pham, S. Ma, B. Space, L. Wojtas, M. Eddaoudi and M. J. Zaworotko, *Nature*, 2013, **495**, 80; (*b*) J. An, S. J. Geib and N. L. Rosi, *J. Am. Chem. Soc.*, 2010, **132**, 38; (*c*) T. Panda, P. Pachfule, Y. Chen, J. Jiang and R. Banerjee, *Chem. Commun.*, 2011, **47**, 2011; (*d*) H.-L. Jiang and Q. Xu, *Chem. Commun.*, 2011, **47**, 3351; (*e*) Q. Lin, T. Wu, S.-T. Zheng, X. Bu and P. Feng, *J. Am. Chem. Soc.*, 2012, **134**, 784; (*f*) W.-Y. Gao, W. Yan, R. Cai, K. Williams, A. Salas, L. Wojtas, X. Shi and S. Ma, *Chem. Commun.*, 2012, **48**, 8898; (*g*) J.-P. Zhang and X.-M. Chen, *J. Am. Chem. Soc.*, 2009, **131**, 5516; (*h*) Y.-X. Tan, Y.-P. He and J. Zhang, *Chem. Commun.*, 2011, **47**, 10647; (*i*) J. Jia, F. Sun, T. Borjigin, H. Ren, T. Zhang, Z. Bian, L. Gao and G. Zhu, *Chem. Commun.*, 2012, **48**, 6010.

3 (*a*) Z. R. Herm, J. A. Swisher, B. Smit, R. Krishna and J. R. Long, *J. Am. Chem. Soc.*, 2011, **133**, 5664; (*b*) Z. R. Herm, R. Krishna and J. R. Long, *Microporous Mesoporous Mater.*, 2012, **151**, 481; (*c*) H. Wu, K. Yao, Y. Zhu, B. Li, Z. Shi, R. Krishna and J. Li, *J. Phys. Chem. C*, 2012, **116**, 16609; (*d*) Y. He, S. Xiang, Z. Zhang, S. Xiong, C. Wu, W. Zhou, T. Yildirim, R. Krishna and B. Chen, *J. Mater. Chem. A*, 2013, **1**, 2543.

4 (*a*) Y. He, Z. Zhang, S. Xiang, H. Wu, F. R. Fronczek, W. Zhou, R. Krishna, M. O'Keeffe and B. Chen, *Chem.–Eur. J.*, 2012, **18**, 1901; (*b*) Y. He, Z. Zhang, S. Xiang, F. R. Fronczek, R. Krishna and B. Chen, *Chem. Commun.*, 2012, **48**, 6493; (*c*) Y. He, S. Xiang, Z. Zhang, S. Xiong, F. R. Fronczek, R. Krishna, M. O'Keeffee and B. Chen, *Chem. Commun.*, 2012, **48**, 10856; (*d*) Z. Guo, H. Wu, G. Srinivas, Y. Zhou, S. Xiang, Z. Chen, Y. Yang, W. Zhou, M. O'Keeffe and B. Chen, *Angew. Chem., Int. Ed.*, 2011, **50**, 3178.

5 M. O'Keeffe, M. A. Peskov, S. J. Ramsden and O. M. Yaghi, *Acc. Chem. Res.*, 2008, **41**, 1782.

6 (*a*) A. L. Myers and J. M. Prausnitz, *AIChE J.*, 1965, **11**, 121; (*b*) R. Krishna and J. R. Long, *J. Phys. Chem. C*, 2011, **115**, 12941; (*c*) E. D. Bloch, W. L. Queen, R. Krishna, J. M. Zadrozny, C. M. Brown and J. R. Long, *Science*, 2012, **335**, 1606; (*d*) Y. He, R. Krishna and B. Chen, *Energy Environ. Sci.*, 2012, **5**, 9107.